What is the Role of Color in Dermoscopy Analysis?

Ana Margarida Caetano Ruela

Under supervision of Professor Jorge dos Santos Salvador Marques

and co-supervision of Professor Teresa Maria de Gouveia Torres Feio Mendonça

ISR, IST, Lisbon, Portugal

***Abstract*—This work aims to contribute for the improvement of Computer-Aided Diagnosis (CAD) systems for melanoma classification. In concrete, the aim of this work is to assess what is the role of color in dermoscopy analysis and to determine which feature extraction method and image descriptor perform best. The assessment was performed by considering a global and a local feature extraction methods along with a rich set of color spaces and color descriptors.**

The best performance ($SE = 100\%$ and $SP = 93\%$) was achieved by both CAD systems using the uni-dimensional color histogram as the image descriptor and images represented in the opponent color space. These results show that color features play a major role in dermoscopy analysis.

Keywords: Skin Lesions, Melanoma, Computer-Aided Diagnosis (CAD) system, Color Features, Feature Extraction, Lesion Classification.

I. Introduction

Melanomas are one of the most life threatening types of cancer. With increased growth rates, melanomas have to be detected in an early stage to get treatment, which only requires the excision of the skin lesion. On the other hand, if melanomas are not treated in their earlier stages they might undergo the metastization process and, as a consequence, the survival rate drops drastically. Thereby, the early detection of melanomas is one of the major concerns of dermatologists.

Melanomas result from an abnormal proliferation of melanocytes. As melanocytes are the cells which produce melanin, the levels of this substance will be increased in these areas. For this reason, melanomas are usually associated with asymmetric lesions, with irregular borders and increased diameters, which show some modifications over time. Furthermore, melanomas are often characterized by the presence of more than one color as well as of some differential structures [1].

Even though melanomas present some specific characteristics, other skin lesions may exhibit some similar features. For this reason, the small dimensions of the lesion and the reflective properties of the skin make it difficult to perform a naked eye diagnosis.

Dermoscopy was an alternative found to naked eye diagnosis. In dermoscopy, dermatologists use a dermatoscope to obtain amplified images of the lesions. Furthermore, it is possible to visualize their morphological structures due to the temporary elimination of the reflective properties of the skin by applying a liquid solution or a cross-polarized light onto the lesion [1].

To aid dermatologists in the diagnosis of dermoscopy images, some medical diagnostic methods were developed. Among these methods, the most popular ones are the ABCD rule of dermoscopy and the 7-point checklist.

The former bases its diagnosis on four lesion properties: asymmetry, border, number of colors and differential structures [1, 2]. The latter is related to the presence or absence or certain differential structures [1, 3].

Nevertheless, the interpretation of dermoscopy images is subjective and, even if performed by experienced dermatologists, may lead to an incorrect or inconclusive diagnosis. For these reasons, Computer-Aided Diagnosis (CAD) systems for melanoma classification have been developed for the last two decades. These systems aim to aid dermatologists in the diagnosis of skin lesions.

II. Previous works

The first CAD system was proposed by A. Green et al. [4] and is divided into three main stages: lesion segmentation, feature extraction and lesion classification. The information extracted from the image was based on the ABCD rule of dermoscopy and comprised shape-, color- and size-related features. In fact, the great majority of the studies mentioned in the literature, developed afterwards, also adopted this model [5–8].

Although in a reduced number, there are also some more recent systems that do not regard lesions as uniforms across all their area. Therefore, instead of using a set of global parameters to describe the lesion, the lesion is divided into blocks, which are considered to be homogeneous and the lesion is represented by a set of local features. The systems developed in [9, 10] adopted this model.

In 2004, Oka et al. [11] developed an Internet-based algorithm, recently updated in [8], which can be used by certified dermatologists all over the world. The system receives a dermoscopy image of a lesion and returns a label. Later on, if the user introduces the histological information about the lesion, the labeled image can be added to the database and used for training.

III. Global and Local classification systems

Two different color-based CAD systems are developed in this work. One of the systems relies on global feature extraction methods to perform image classification, whereas the other bases its decision on local color features. In the former, lesions are assumed to be homogeneous and can be described by a set of global parameters. In the latter, lesions are considered to be non-uniform. Therefore, they are divided into patches which are considered to be uniform. The division of the lesion, extraction of local features and representation of the images is based one the Bag-of-Features (BoF) model. Figure 1 shows an overall description of the global (a) and local (b) classification systems.

IV. Global system

The global system (see Figure 1 a) has three main stages: image segmentation, feature extraction and lesion classification. In the first stage, the system receives a dermoscopy image as an input. Each dermoscopy image is a discrete color image defined as $I : \Omega \rightarrow \mathbb{Z}^3$, where Ω is a subset of $\mathbb{Z}^2$ and each point of the image is defined by $(p_1, p_2) \in \Omega$. Each point (p_1, p_2) corresponds to a tridimensional vector in which each coordinate provides information regarding a color channel. In this stage, the region of the lesion, of the input image, is separated from the healthy skin. The segmentation is performed by using a binary image (segmentation mask) whose active pixels define the lesion (R). These segmentation masks were manually obtained under the supervision of an experienced dermatologist.

Thereafter, R is divided into two disjoint regions: an inner region (R_1) and the border (R_2). In the feature extraction stage, features are extracted from four different lesions: R, R_1, R_2 and the concatenation of the last two ($R_1 + R_2$). These regions are represented in Figure 2.

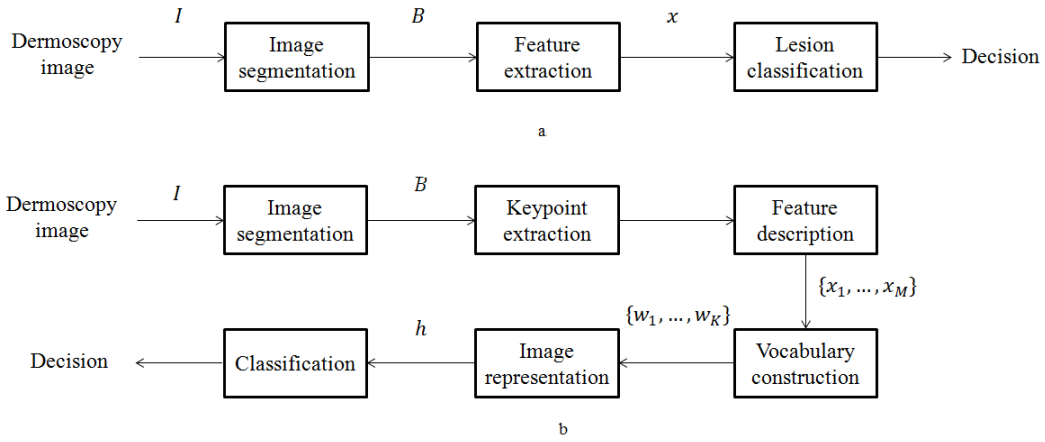

Figure 1: Overall description of the CAD systems for lesion classification by (a) using global features and (b) local features.

At last, in the lesion classification stage, Adaboost [12] and the k-Nearest Neighbors (k-NN) [13] are, separately, trained to distinguish melanomas from non-melanomas.

Figure 2: Representation of regions R_1 (red) and R_2 (yellow) on the left, and region R on the right.

V. Local system

The local system is a little bit more complex and is divided into six main stages: (1) image segmentation, (2) keypoint extraction, (3) feature description, (4) vocabulary construction, (5) image representation and (6) classification. The former and the latter are the same of the global system, the remaining are described as follows:

Keypoint extraction: In this stage, a set of keypoints is obtained using the nodes of a regular grid of points defined on the image (regular grid detection method). Each image patch ($\delta \times \delta$ pixels), is defined by the keypoint in the center and its surrounding pixels. Since we are only interested in the regions of the image which contain the lesion, the blocks which do not have a significant overlap with the lesion ($< 50\%$) are discarded. Figure 3 shows an example of a lesion and the correspondent valid patches.

Feature description: In this stage, each region j of an image i is described by a local descriptor and represented by a feature vector $x_j^{(i)} \in \mathbb{R}^d$.

After the process of feature description, an image i is represented as follows

$$\mathbf{X}^{(i)} = \left[x_1^{(i)}, x_2^{(i)}, ..., x_{M^i}^{(i)}\right], x_j^{(i)} \in \mathbb{R}^d \qquad (1)$$

where $M^{(i)}$ is the total number of regions of image i.

Vocabulary construction: The vocabulary construction only occurs during the training phase. In this stage all local features of all the training images are put together and are represented by $\mathbf{G}$ as follows

$$\mathbf{G} = \left[\mathbf{X}^{(1)}, \mathbf{X}^{(2)}, ..., \mathbf{X}^{(N)}\right], \qquad (2)$$

where N is the number of training images. The visual vocabulary is constructed by using the k-means clustering algorithm which will select K prototypes to represent all the visual features extracted from the training images. Each one of these prototypes represents

a visual word, $w \in \mathbb{R}^d$.

Image representation: Images are represented by using histograms of visual words. Each test image undergoes all the previous stages except the vocabulary construction. The vocabulary used is the one computed during the training phase. Each bin of the histogram represents a visual word from this vocabulary. The histograms are computed as follows. Firstly, each feature vector, $x_j^{(i)}$, of image i is associated to its most similar visual word w_k that satisfies

$$d_E(w_k, x_j^{(i)}) \leq d_E(w_l, x_j^{(i)}), \forall l = 1, ..., M^{(i)}. \quad (3)$$

where d_E is the Euclidean Distance (ED) between w_k and $x^{(i)}$, and $M^{(i)}$ is the number of valid patches of image $I^{(i)}$.

Let $w_j^{(i)}$ be the closest visual feature of $x_j^{(i)}$, the intensity of the bin representing w_l is given by

$$n(w_l|I^i) = \sum_{j=1}^{M^{(i)}} \delta(w_l - w_j^{(i)}), \quad (4)$$

where,

$$\delta(p) = \begin{cases} 1, & \text{if } p = 0 \\ 0, & \text{if } p \neq 0 \end{cases}. \quad (5)$$

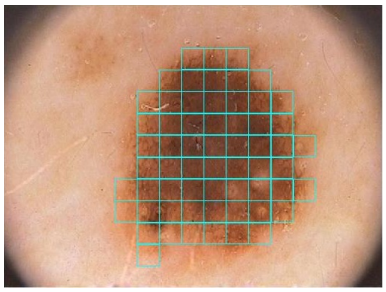

Figure 3: Example of a lesion and respective valid patches.

VI. Color Features

Color has played an important role in dermoscopy analysis. Previously to CAD systems, color was already used by dermatologists for melanoma classification in techniques such as the ABCD rule. The greater the number of colors present in the lesion, the greater is the chance of being a melanoma. Furthermore, color-based features have been used to represent the lesions in all the CAD systems mentioned in the literature [4–8, 10, 14–17]. However, the great majority of these systems only uses simple features such as the mean and variation of the color channels.

Furthermore, most systems only consider the images represented in the RGB color space. The RGB color space has some undesirable characteristics such as a high correlation between channels and a perceptual non-uniformity. Therefore, in this work, in addition to the RGB color space, six other color spaces were used: HSV, HSL, HSI, Opponent Color Space (O1/2/3), $L^*a^*b^*$ and L^*uv. All except the O1/2/3 color space had already been used in CAD systems for melanoma classification [7, 8, 14, 16]. The color spaces discussed in this section can be divided into two distinct groups [18]: the ones derived from the human visual system (RGB, HSV, HSL, HSI and Opponent Color Space (O1/2/3)) and the ones derived from the Commission Internationale de L'Eclairage (CIE) color spaces ($L^*a^*b^*$ and L^*uv).

In this section the color descriptors used in these systems are described. Four color descriptors are used: the Unidimensional Color Histogram (UCH), the Tridimensional Color Histogram (TCH), the Generalized Color Moments (GCM) and the Mean Color Vector (MCV). The UCH and the GCM are used in both systems. The TCH, however, is not used in the local system because it would lead to a very time consuming feature description process. Instead, we chose to use the MCV. This descriptor contains the simplest features which can be used to define a patch.

A. Color Histograms

Color histograms provide information about the color probability distribution in each image. They are obtained by splitting the color range into disjoint bins and measuring the number of times a pixel color falls in each bin. Since they do not provide any information regarding the spatial color distribution, they are rotation and translation invariant. Moreover, color histograms are not significantly affected by changes in the image scale, partial occlusions and to blurred regions [19].

Images can be described by uni-, bi- and tridimensional histograms according to the number of color channels used to compute them. In this work, only unidimensional and tridimensional color histograms are used as image descriptors and they are, respectively, computed as follows

$$h_c(i) = \sum_{(p_1,p_2)\in\mathbb{Z}^2} b_i^c(I_c(p_1,p_2)), i = 1, ..., N_c, \quad (6)$$

and

$$\begin{aligned} h(i,j,k) = \textstyle\sum_{(p_1,p_2)\in\mathbb{R}^2} b_i^1(I_1(p_1,p_2)) \\ \times b_j^2(I_2(p_1,p_2)) \times b_k^3(I_3(p_1,p_2)), \end{aligned} \quad (7)$$

where $c = \{1, 2, 3\}$ corresponds to the color channel, $I_c(p_1, p_2)$ is the intensity of pixel (p_1, p_2) in c and $b_i^c(I)$ is the characteristic function of the i^{th} bin of channel c.

$$b_i^c(I_c(p_1,p_2)) = \begin{cases} 1 & I_c(p_1,p_2) \in i^{th} \text{ bin of } c \\ 0 & \text{otherwise} \end{cases} \quad (8)$$

Afterwards, the histograms are normalized so that the sum of their elements equals 1.

B. Generalized color moments

The generalized color moments are also potentially good descriptors because in addition to the color information they also provide some spatial information. They were proposed by Mindru et al [20], in 1999, and are computed as follows

$$\begin{aligned} M_{pq}^{abc} = \textstyle\int\int_R p_1^p \times p_2^q \times [I_1(p_1,p_2)]^a \\ \times [I_2(p_1,p_2)]^b \times [I_3(p_1,p_2)]^c dp_1 dp_2, \end{aligned} \quad (9)$$

where M_{pq}^{abc} is the moment of order $p+q$ and degree $a+b+c$. Only moments of order up to or equal to 1 and degree up to or equal to 2 are considered to avoid the instability provided by moments of higher order and/or degree.

It is not fair to compare the moments between lesions with different sizes. Therefore, to guarantee scale invariance, this expression undergoes the following transformation

$$(M_{pq}^{abc})' = \frac{M_{pq}^{abc}}{\#Q^{1+\frac{p+q}{2}}}, \quad (10)$$

where $\#Q$ is the number of pixels within region R.

C. Mean color vector

A mean color vector is a vector containing the mean intensities of the three color channels. Let $I_c(p_1, p_2)$ be the intensity of pixel (p_1, p_2) of channel c, the mean intensity of the channel is given by:

$$f_c = \frac{\sum_{p_1=i}^{\delta_i+i} \sum_{p_2=j}^{\delta j+j} I_c(p_1,p_2)}{\delta_i \times \delta j}, \quad (11)$$

where δ_i and δ_j represent the patch dimensions. Therefore, the descriptor $x \in \mathbb{R}^3$ is a vector containing the three mean values.

VII. Results

In this section we will analyze the results obtained by both global and local systems.

A. Dataset

The dataset used in this work contains dermoscopy images collected from the database of Hospital Pedro

Hispano, in Matosinhos. This dataset comprises 148 melanocytic lesions: 14 melanomas ($\approx$ 9%) and 134 non-melanomas ($\approx$ 91%). The images were obtained by using a dermatoscope with an amplification of 20× during routine clinical examinations.

The images were compressed into the JPEG format. Each image is represented in the RGB color space and, thus, is composed by three channels, one for each primary. Each color channel contains information about the intensity distribution of that color throughout the image.

Image classification was performed by an experient dermatologist and, in most cases, the diagnosis was confirmed by histological examination.

The images' pre-processement included hair and reflection removal. Hair removal was performed by using directional filters, whereas reflection removal was performed by using a thresholding algorithm. The gaps caused by the artifacts removal were filled by using an inpainting algorithm [21].

B. Evaluation Metrics

The performance of each system was assess by using leave-one-out or 10-fold cross validation, according to the complexity and time consumption of the task. This performance was evaluated by computing the Sensitivity (SE) and Specificity (SP) of the system. In order to determine which system performs best, a cost function was established. In the context of this problem, having a false negative has a higher cost than having a false positive, because the misdiagnosis of a melanoma delays a possible treatment and decreases the patient's survival chances. In this work, we considered that the misdiagnosis of a melanoma costs two times more than the misdiagnosis of a non-melanoma. The cost function used in this work is given by

$$C_T = 1 - \frac{2}{3} \times SE - \frac{1}{3} \times SP. \quad (12)$$

C. Optimization of parameters

1) Global system: The global classification system was tested by using all possible combinations between three types ofdescriptors (UCH, TCH and GCM), seven color spaces (RGB, HSV, HSL, HSI, O1/2/3, L*a*b* and L*uv) and two classifiers (k-NN and AdaBoost).

In each system, in order to optimize the largest possible set of parameters, multiple configurations were tested. Among these parameters one has the region from which features are extracted (R, R_1, R_2 and $R_1 + R_2$) and the number of bins of both UCH (15 to 50 bins) and TCH ($\{5 \times 5 \times 5, 10 \times 10 \times 10, 15 \times 15 \times 15, 20 \times 20 \times 20\}$. Regarding k-NN, both the number of nearest neighbors ($k \in \{5,\ 7, 9,\ 11, 13,\ 15, 17,\ 19, 21,\ 23\}$) and the distance used to compute the similarity between the vectors (ED, Histogram Intersection (HI), Kullback-Leibler Divergence (KLD)) were optimized [1] Lastly, concerning AdaBoost, optimization was performed for both the weight given to the positive class ($\alpha \in \{1, 2\}$) and the number of weak classifiers ($T \in \{2, 5, 10, 20\}$).

The best performance obtained by each descriptor and by each classifier as well as the used parameters are presented in Table I. The best result ($SE = 100\%$ and $SP = 93\%$) was achieved by using UCH of 42 bins, in the O1/2/3 color space, as the image descriptor and kNN as the classifier. Furthermore, the concatenation of the features extracted from regions R_1 and R_2 proved to lead to the best result. Regarding the classifier, the 5-NN performed best by using the ED as the similarity measure.

[1]Except for the system using GCM as the descriptor, in this case only ED was used to compute the distance between feature vectors. HI and KLD are only applicable to histograms.

kNN - Global								
Descriptor	**Color Space**	**SE**	**SP**	**Cost**	**Region**	**Number of bins**	**Distance**	**k**
UCH	O1/2/3	100	93	0.02	$R_1 + R_2$	42	ED	5
TCH	L*a*b*	93	91	0.08	R_2	125	KLD	19
GCM	RGB	93	93	0.07	R	-	HI	19
AdaBoost - Global								
Descriptor	**Color Space**	**SE**	**SP**	**Cost**	**Region**	**Number of bins**	α	**T**
UCH	O1/2/3	100	85	0.05	R_2	41	1/2	2
TCH	L*a*b*	93	92	0.08	$R_1 + R_2/R_1/R$	10×10×10	1	2
	HSV	93	92	0.08	$R_1 + R_2/R_1$	10×10×10	1	2
GCM	L*a*b*	93	89	0.08	R/R_1	-	1	2

Table I: Best performance of each global system and the respective best configuration.

2) Local system: Similarly to the global system, the local system was tested by using three descriptors (UCH, GCM and MCV), seven color spaces (RGB, HSV, HSL, HSI, O1/2/3, L*a*b* and L*uv) and two classifiers (kNN and AdaBoost).

In this system the optimized parameters were: the size of the patches $\delta \times \delta$ ($\delta \in \{20, 40\,60, 80, 100\}$), the size of the visual vocabulary ($K \in \{50\,, 100, 150, 200\}$) and the number of bins of the UCH ($\{5, 10\,, 15, 20, 25, 30\}$). Furthermore, the optimization of kNN and AdaBoost was performed regarding the same parameters mentioned in the previous section.

Table II shows the best performance achieved by each system and each classifier as well as the used parameters. The best performance was once again achieved by using the UCH in the O1/2/3 color space as the image descriptor. However, in this system AdaBoost performed a better classification than k-NN. In this configuration the image patches were defined by using a $\delta = 60$ and 100 visual words. Regarding Adaboost, it performed best by assigning the double of the weight to melanomas ($\delta = 2$) and by using 10 weak classifiers.

VIII. Comparison between the global and local systems

Tables I and II show respectively the best performance achieved by the global and local systems for each descriptor and classifier

Interestingly, the best performance ($SE = 100\%$ and $SP = 93\%$) was reached by both systems. Furthermore, they were both able to achieve this result by using the unidimensional color histogram O1/2/3 color space as the color descriptor.

It had already been stated that color histograms are powerful descriptors and, thus, the good results they achieved did not come as a surprise. Concerning the color space, it is also not surprising that the best performance has been achieved by using the images in the O1/2/3 color space [22], because from all these color representations this is the most similar to the second stage of the two stage color vision model [23]. Hence, this representation is the closest to the representation of color in the human brain. This possibly explains why the classification by using images in the O1/2/3 better mimic the decision of a dermatologist.

In general, the systems based on a local feature extraction method were able to reach better performances despite the simplicity of some of the used descriptors, such as the mean color vector. However, the systems based on the global feature extraction method has the advantage of being simpler to implement and less time consuming. Therefore, there is a trade-off between simplicity and performance.

Nevertheless, in the context of this work, where the patients' health and survival chances are at stake, per-

kNN - Local									
Descriptor	**Color Space**	**SE**	**SP**	**Cost**	**K**	δ	**Number of bins**	**Distance**	**k**
UCM	O1/2/3	100	90	0.03	50	80	25	HI	5
MCV	L*a*b*	100	74	0.09	200	60	-	KLD	11
GCM	HSL	100	89	0.04	100/150	20	-	HI/KLD	21/11
AdaBoost - Local									
Descriptor	**Color Space**	**SE**	**SP**	**Cost**	**K**	δ	**Number of bins**	α	**T**
UCH	O1/2/3	100	93	0.02	100	60	30	2	10
MCV	L*a*b*	93	95	0.06	200	20	-	2	10
GCM	HSL	100	91	0.03	200	20	-	1	2

Table II: Best performance of each local system and the respective best configuration.

formance must have the greater weight.

Figures 4 and 5 show some examples of True Negatives (TNs) (top row, left), False Negatives (FNs) (down row, left) and TPs (down row, right) images, classified by using these best configurations. Both systems accurately classified all melanomas and failed to classify 10 out of the 134 non-melanomas. From the 10 misclassified lesions, 5 were misclassified by both. These 5 lesions are showed in Figure 6.

IX. Conclusions and Future work

The aim of this work was to assess what is the role of color features in the classification of melanomas. In order to reach this goal, two different CAD systems, whose classification is solely based on color features, were developed. The main difference between the systems is at the feature extraction level. One of the systems uses a global feature extraction method whereas the other adopts a local one.

Both systems were able to achieve a configuration which lead to a SE of 100% and a SP of 93%. Interestingly, both systems reached this result by using the UCH in the O1/2/3 color space as the image descriptor. These findings allow us to draw some conclusions. Firstly, it becomes clear that color-based features play a major role in dermoscopy analysis. Secondly, the UCH in the O1/2/3 is a promising color descriptor which should be studied in more detail and incorporated in future CAD systems.

Regarding which feature extraction method performs best the conclusion is not as straightforward as the others. Both methods were able to originate a system which lead to the best performance. However, in general, the local system achieved better results.

Both of the systems developed in this work can be further tested and further improved. In the future, the systems should be tested with a larger and more balanced database. It would also be interesting to use other classifiers, such as the Artificial Neural Networks (ANN) and the Support Vector Machines (SVM), which have already led to good performances in other systems [5, 7]. Furthermore, the best color features should be combined with other types of features, such as shape- and texture-based features in future CAD systems.

X. Aknowlegdments

This work is integrated in the project PTDC/SAUBEB/103471/2008, funded by FCT. The author would like to thank Professors Jorge Salvador Marques and Teresa Mendonça for the opportunity to work in this project and for the guidance and support provided in this work. The author also wants to acknowledge Catarina Barata for her valuable help.

The dermoscopic images used in this work were kindly provided by Dr. J. Rozeira from Hospital Pedro Hispano.

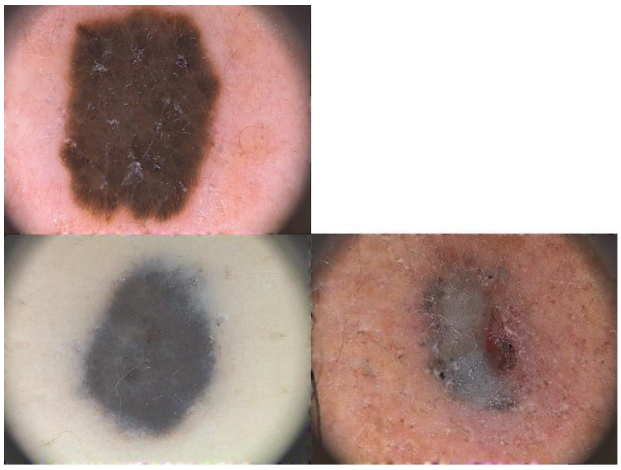

Figure 4: Examples of images classified by the best global system: a TN (top row, left), FN (down row, left) and TP (down row, right). There was no FP classification.

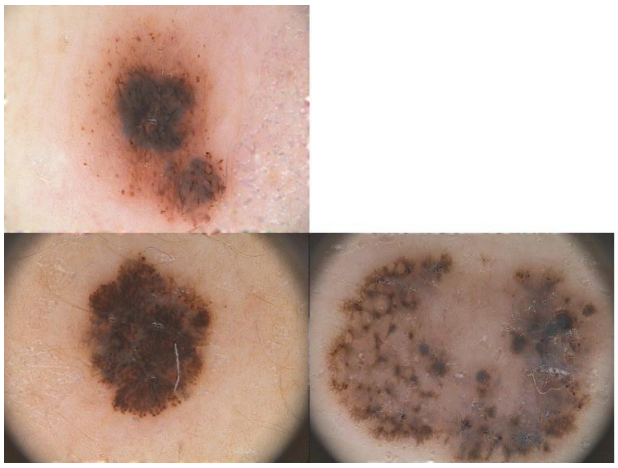

Figure 5: Examples of images classified by the best local system: a TN (top row, left), FN (down row, left) and TP (down row, right). There was no FP classification.

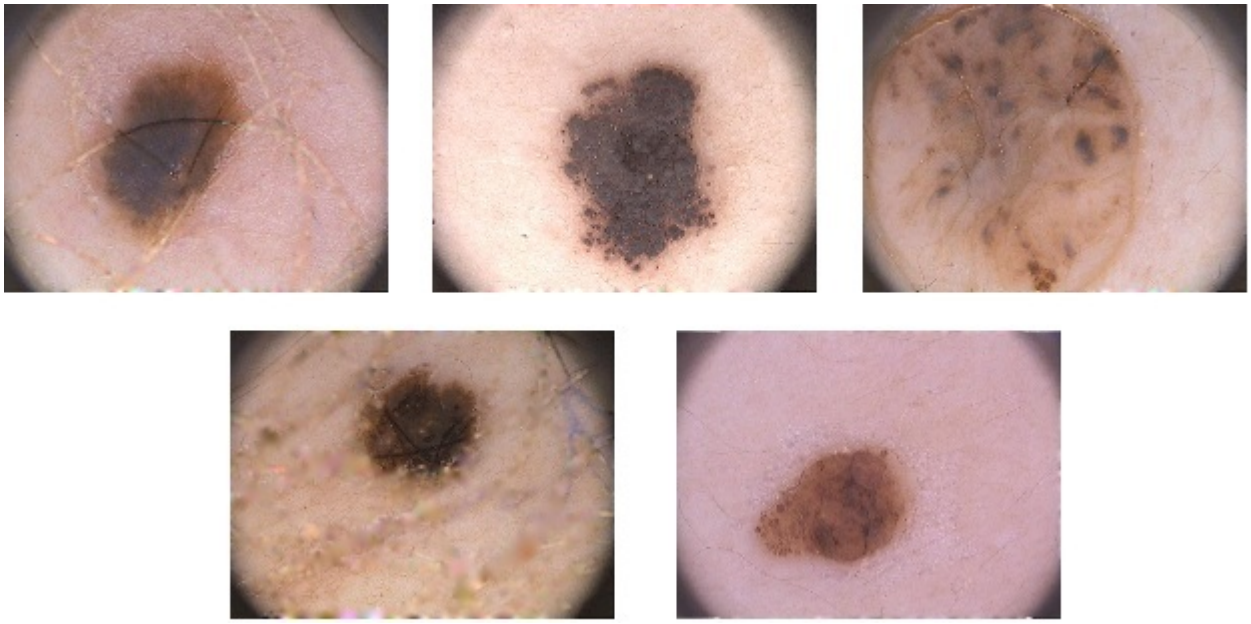

Figure 6: False Positives detected by the best configuration of both global and local systems.

References

[1] "Dermoscopy," http://www.dermoscopy.org/.

[2] F. Nachbar, W. Stolz, T. Merkle, A. B. Cognetta, T. Vogt, P. Landthaler, M. Bilek, O. Braun-Falco, and G. Plewig, "The abcd rule of dermatoscopy. high prospective value in the diagnosis of doubtful melanocytic skin lesions," *J Am Acad Dermatol*, vol. 30, no. 4, pp. 551–559, April 1994.

[3] G. Argenziano, G. Fabbrocini, C. P., V. De Giorgi, E. Sammarco, and M. Delfino, "Epiluminescence microscopy for the diagnosis of doubtful melanocytic skin lesions. comparison of the abcd rule of dermatoscopy and a new 7-point checklist based on pattern analysis," *Arch Dermatol*, vol. 134, pp. 1563–1570, 1998.

[4] A. Green, N. Martin, G. McKenzie, J. Pfitzner, F. Quintarell, B. W. Thomas, M. O'Rourk, and N. Knight, "Computer image analysis of pigmented skin lesions," *Melanoma Research*, vol. 1, pp. 231–236, 1991.

[5] P. Rubegni, G. Cevenini, M. Burroni, R. Perotti, G. Dell'Eva, P. Sbano, C. Miracco, P. Luzi, P. Tosi, P. Barbini, and L. Andreassi, "Automated diagnosis of pigmented skin lesions," *International Journal of Cancer*, vol. 101, pp. 576–580, 2002.

[6] K. Hoffmann, T. Gambichler, A. Rick, M. Kreutz, M. Anschuetz, T. Gruumlnendick, A. Orlikov, S. Gehlen, R. Per-

otti, L. Andreassi, J. Newton Bishop, J.-P. Césarini, T. Fischer, P. J. Frosch, R. Lindskov, R. Mackie, D. Nashan, A. Sommer, M. Neumann, J. P. Ortonne, P. Bahadoran, P. F. Penas, U. Zoras, and P. Altmeyer, "Diagnostic and neural analysis of skin cancer (danaos). a multicentre study for collection and computer-aided analysis of data from pigmented skin lesions using digital dermoscopy," *British Journal of Dermatology*, vol. 149, pp. 801–809, 2004.

[7] M. E. Celebi, H. A. Kingravi, B. B. Uddin, H. Iyatomi, A. Y. A, W. V. Stoecker, and R. H. Moss, "A methodological approach to the classification of dermoscopy images," *Computerized Medical Imaging and Graphics*, vol. 31, no. 6, pp. 362–371, 2007.

[8] H. Iyatomi, M. E. Celebi, H. Oka, and M. Tanaka, "An improved internet-based melanoma screening system with dermatologist-like tumor area extraction algorithm," *Computerized Medical Imaging and Graphics*, vol. 32, pp. 566–579, 2008.

[9] S. Seidenari, G. Pellacani, and C. Grana, "Pigment distribution in melanocytic lesion images: a digital parameter to be employed for computer-aided diagnosis," *Skin Research and Technology*, vol. 11, pp. 236–241, 2005.

[10] N. Situ, T. Wadhawan, R. Hu, K. Lancaster, X. Yuan, and G. Zouridakis, "Evaluating sampling strategies of dermoscopic interest points," in *ISBI'11*, 2011, pp. 109–112.

[11] H. Oka, M. Hashimoto, H. Iyatomi, G. Argenziano, H. Soyer, and M. Tanaka, "Internet-based program for automatic discrimination of dermoscopic images between melanomas and clark naevi," *British Journal of Dermatology*, vol. 150, no. 5, pp. 1041–1041, 2004.

[12] Y. Freund and R. E. Schapire, "A decision-theoretic generalization of on-line learning and an application to boosting," *J. Comput. Syst. Sci.*, vol. 55, no. 1, pp. 119–139, August 1997.

[13] R. Duda, P. Hart, and D. Stork, *Pattern classification and scene analysis. Part 1, Pattern classification*, ser. Pattern Classification and Scene Analysis: Pattern Classification. Wiley, 2001.

[14] F. Ecral, A. Chawla, W. V. Stoecker, H.-C. Lee, and R. H. Moss, "Neural network diagnosis of malignant melanoma from color images," *IEEE Transactions on Biomedical Engineering*, vol. 41, no. 9, pp. 837–845, September 1994.

[15] L. Andreassi, R. Perotti, P. Rubegni, M. Burroni, G. Cevenini, M. Biagioli, P. Taddeucci, G. Dell'Eva, and P. Barbini, "Digital dermoscopy analysis for the differentiation of atypical nevi and early melanoma: a new quantitative semiology," *Archives of Dermatological Research*, vol. 135, pp. 1459–1465, 1999.

[16] H. Ganster, A. Pinz, R. Rohrer, E. Wildling, M. Blinder, and K. H., "Automated melanoma recognition," *IEEE Transactions on Biomedical Engineering*, vol. 20, no. 3, pp. 233–239, March 2001.

[17] A. Blum, H. Luedtke, U. Ellwanger, R. Schwabe, G. Rassner, and C. Garbe, "Digital image analysis for diagnosis of cutaneous melanoma. development of a highly effective computer algorithm based on analysis of 837 melanocytic lesions," *British Association of Dermatologists*, vol. 151, pp. 1029–1038, 2004.

[18] M. Tkalcic and J. Tasic, "Colour spaces - perceptual, historical and applicational background," *Proc. Eurocon 2003*, pp. 304–308, September 2003.

[19] M. J. Swain and D. H. Ballard, "Color indexing," *International Journal of Computer Vision*, vol. 7, no. 1, pp. 11–32, September 1991.

[20] F. Mindru, T. Moons, and L. V. Gool, "Recognizing color patterns irrespective of viewpoint and illumination," 1999, pp. 368–373.

[21] C. Barata, J. S. Marques, and J. Rozeira, "A system for the detection of pigment network in dermoscopy images using directional filters," *Biomedical Engineering, IEEE Transactions on*, vol. 59, no. 10, pp. 2744–2754, oct. 2012.

[22] H. Palus, *Colour spaces*. Chapmann and Hall, 1998.

[23] W. Frei and B. Baxter, "Rate-distortion coding stimulation for color images," *IEEE Transactions on Systems, Man, and Cybernetics*, vol. COM-25, no. 11, pp. 1385–1392, November 1977.